

Journal of Biomedical Optics

SPIEDigitalLibrary.org/jbo

Accurate measurement of volume and shape of resting and activated blood platelets from light scattering

Alexander E. Moskalensky
Maxim A. Yurkin
Anastasiya I. Konokhova
Dmitry I. Strokotov
Vyacheslav M. Nekrasov
Andrei V. Chernyshev
Galina A. Tsvetovskaya
Elena D. Chikova
Valeri P. Maltsev

Accurate measurement of volume and shape of resting and activated blood platelets from light scattering

Alexander E. Moskalensky,^{a,b} Maxim A. Yurkin,^{a,b} Anastasiya I. Konokhova,^{a,b} Dmitry I. Strokotov,^{a,b} Vyacheslav M. Nekrasov,^{a,b} Andrei V. Chernyshev,^{a,b} Galina A. Tsvetovskaya,^{c,d} Elena D. Chikova,^{b,c,d} and Valeri P. Maltsev^{a,b}

^aInstitute of Chemical Kinetics and Combustion SB RAS, Institutskaya 3, 630090, Novosibirsk, Russia

^bNovosibirsk State University, Pirogova 2, 630090, Novosibirsk, Russia

^cANO "Center of New Medical Technologies in Akademgorodok," Pirogova 25/4, 630090, Novosibirsk, Russia

^dInstitute of Chemical Biology and Fundamental Medicine, Lavrentiev Avenue 8, 630090, Novosibirsk, Russia

Abstract. We introduce a novel approach for determination of volume and shape of individual blood platelets modeled as an oblate spheroid from angle-resolved light scattering with flow-cytometric technique. The light-scattering profiles (LSPs) of individual platelets were measured with the scanning flow cytometer and the platelet characteristics were determined from the solution of the inverse light-scattering problem using the precomputed database of theoretical LSPs. We revealed a phenomenon of parameter compensation, which is partly explained in the framework of anomalous diffraction approximation. To overcome this problem, additional *a priori* information on the platelet refractive index was used. It allowed us to determine the size of each platelet with subdiffraction precision and independent of the particular value of the platelet aspect ratio. The shape (spheroidal aspect ratio) distributions of platelets showed substantial differences between native and activated by 10 μM adenosine diphosphate samples. We expect that the new approach may find use in hematological analyzers for accurate measurement of platelet volume distribution and for determination of the platelet activation efficiency. © 2013 Society of Photo-Optical Instrumentation Engineers (SPIE). [DOI: 10.1117/1.JBO.18.1.017001]

Keywords: blood platelets; cells; flow cytometry; inverse problems; scattering.

Paper 12425 received Jul. 5, 2012; revised manuscript received Dec. 5, 2012; accepted for publication Dec. 7, 2012; published online Jan. 3, 2013.

1 Introduction

Blood platelets play a central role in hemostasis and are involved in many pathophysiological processes, including thrombosis, hemorrhage, inflammation, and cancer.¹ The main function of platelets is the formation of hemostatic plugs in response to the vessel wall injury. This is achieved by platelet activation as soon as subendothelium is exposed, followed by platelet aggregation and adhesion to the damaged area.

Unactivated (resting) platelets circulate in blood as small disc-shaped cells without nuclei. Their average dimensions as measured by scanning electron microscopy are 3 (diameter) \times 1 μm^2 (thickness).^{2,3} Similar results were obtained with phase-contrast microscopy.⁴ Rigorous comparison of phase-contrast microscopic measurements with other data showed that an oblate spheroid is a suitable optical model for a platelet.⁵ It was also shown that aspect ratio (diameter/thickness) varies from cell to cell within a wide range from 2 to 8.

Blood platelets are also very heterogeneous in size.⁶ Platelet volume distribution as obtained with resistive-particle counting (Coulter method) shows log-normality with cells ranging from 2 to 15 fl.^{7,8} These measurements are approximate because cell shape can affect the measured platelet volume by a factor of 3.⁹ However, such distribution is now routinely measured during the complete blood count and mean platelets volume (MPV) and platelets distribution width (PDW) are considered clinically important parameters.¹⁰

As mentioned above, platelet activation is the first step in formation of thrombi, which implies diagnostic value of assessment of this activation. Tests for detection of activated platelets using specific monoclonal antibodies and flow cytometry are now available,^{11,12} measuring a fraction of *in vivo* activated platelets.¹³ Studies of *in vitro* platelets response to agonists, such as adenosine diphosphate (ADP) or thrombin, are also of interest.¹⁴

Flow-cytometric forward versus side light-scattering maps (FSC-SSC) for resting and activated platelets differ only slightly,¹⁵ although a platelet undergoes dramatic shape change, becoming a spiny sphere with pseudopodia.¹⁶ Excluding pseudopodia, an activated platelet can, therefore, be described as spheroid with aspect ratio slightly larger than 1. For example, quantitative study with phase-contrast microscopy showed that mean aspect ratio of platelets decreases from 3 to 1.25 during activation by 10 μM ADP.¹⁷ Another study¹⁸ assessed rabbit platelets shape change with electron microscopy and gave similar results.

Scanning flow cytometer (SFC) is capable of measuring angle-resolved light-scattering pattern (LSP) of individual particles in flow¹⁹ in addition to ordinary flow-cytometric FSC and SSC amplitudes. An analysis of the LSP potentially allows one to determine morphological characteristics of biological particles.²⁰ However, such characterization constitutes the inverse light-scattering problem, which is a field of active research, see e.g., Refs. 21 and 22. The only reported application of this approach to platelets²³ have two serious drawbacks. First, an ethylenediaminetetraacetic acid (EDTA) was used as anticoagulant,

Address all correspondence to: Valeri Maltsev, Institute of Chemical Kinetics and Combustion SB RAS, Institutskaya 3, 630090, Novosibirsk, Russia and Novosibirsk State University, Pirogova 2, 630090, Novosibirsk, Russia. Tel: +73833333240; Fax: +73833307350; E-mail: maltsev@kinetics.nsc.ru

which induces platelets swelling resulting in spherizing of cells.²⁴ In particular, this simplifies both calculation of LSPs and solution of the inverse light-scattering problem. Second, the simplest characterization method was used with no assessment of uncertainties of determined cell characteristics.

The goal of this paper is two-fold. First, we develop a general approach to characterize nonspherical particles from the LSPs measured with the SFC, using the database of theoretical LSPs. Second, we apply this approach to blood platelets to create a rigorous method of their characterization (both resting and activated cells) avoiding the abovementioned drawbacks. After describing materials and methods in Sec. 2, we develop the general approach to characterization in Sec. 3, as well as specific application to blood platelets. Section 4 is devoted to theoretical analysis of different aspects of light scattering by platelets. In Sec. 5 we illustrate the performance of a new method of platelet characterization on a sample of blood from a healthy donor. Section 6 concludes the paper, discussing current limitations and directions for future research.

2 Materials and Methods

2.1 Sample Preparation

Blood was taken from a healthy donor by venipuncture and collected in a vacuum tube containing sodium citrate as anticoagulant (9:1 blood to sodium citrate). Within 1 h of the collection, platelet plasma was obtained by centrifugation at 900 g for 15 min at room temperature. The sample was 100-fold diluted in 0.9% saline, and 1 and 2 μm polystyrene microspheres (Molecular Probes, USA) were added for a scaling of the SFC optics. Part of this sample was immediately analyzed with the SFC measuring the LSPs of all particles in the sample, including platelets and other constituents of blood plasma. Another part was stimulated by the addition of 10 μM ADP, delayed for 1 min, and then analyzed with the SFC. It is important to note that the dilution greatly reduced platelet aggregation; therefore, stimulation by ADP resulted only in activation of platelets.

We plot all measured particles on a map of LSP integrated from 10 deg to 60 deg (see Sec. 2.2) versus LSP integrated from 10 deg to 11 deg (Fig. 1). This is analogous to the SSCxFSC map used in ordinary flow cytometers. The clusters corresponding to polystyrene 1 μm microspheres and their dimers are

clearly visible; they define gates G1, G2, and G3. A characteristic area of blood platelets is also visible and define gate G4. After the addition of ADP, the area of platelets narrows in agreement with ordinary flow-cytometric experiments.¹⁵ However, we used the same gate G4 for identification of platelets after activation.

2.2 Scanning Flow Cytometer

Technical features of the SFC and the operational function of the optical cell were previously described in detail elsewhere.²⁵ The actual SFC was fabricated by the Cytonova Ltd. company (Novosibirsk, Russia, <http://cyto.kinetics.nsc.ru/>). It is equipped with a 40 mW laser of 660 nm (LM-660-20-S) for generation of LSPs of individual particles. Another 15 mW laser of 488 nm (Uniphase 2214-12SLAB) is used for generation of the trigger signal. The measured LSP is as follows:

$$I(\theta) = \frac{1}{2\pi} \int_0^{2\pi} [S_{11}(\theta, \varphi) + S_{14}(\theta, \varphi)] d\varphi, \quad (1)$$

where S is the Mueller matrix,²⁶ and θ and φ are polar and azimuth scattering angles. The operational polar angular range of the SFC was determined from the analysis of polystyrene microspheres, as described in Ref. 21, to be from 10 deg to 60 deg. Measurement time for one particle in a flow is less than 1 ms, which allows us to neglect particle rotation. Due to the axial symmetry of the optical system of the SFC, the measured LSP depends only on the polar orientation angle Ψ of the particle (Fig. 2).

2.3 Light-Scattering Simulations

We use an oblate spheroid as an optical model of a blood platelet. With regard to LSP calculation this model has four parameters, which we chose to be an equi-volume sphere radius r , an aspect ratio ε , a refractive index n , and an orientation angle Ψ (Fig. 2).

Theoretical LSPs for oblate spheroids were calculated using the discrete dipole approximation (DDA).²⁷ In particular, we used open-source code ADDA v.1.0.²⁸ The LSPs of platelets were simulated for θ ranging from 10 deg to 70 deg with a step of 1 deg. We used 12 dipoles per a wavelength of incident

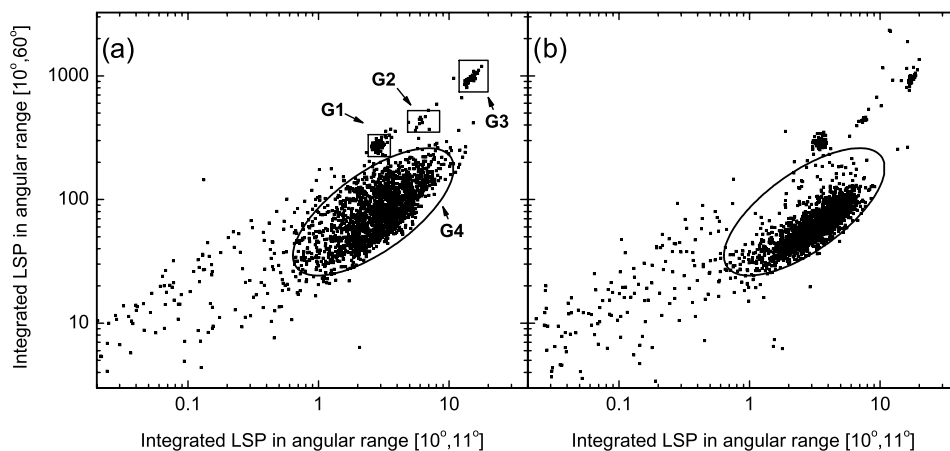


Fig. 1 The scatter plot of the integrated LSP in the angular range [10 deg, 60 deg] versus that in the range [10 deg, 11 deg] in log-log scale for (a) the native sample and (b) the sample treated by 10 μM ADP. Polystyrene microspheres of 1 and 2 μm are gated by G1 and G3, respectively, while dimers of 1 μm polystyrene microspheres are gated by G2. Events in G4 (selected for further processing) are mainly formed by blood platelets.

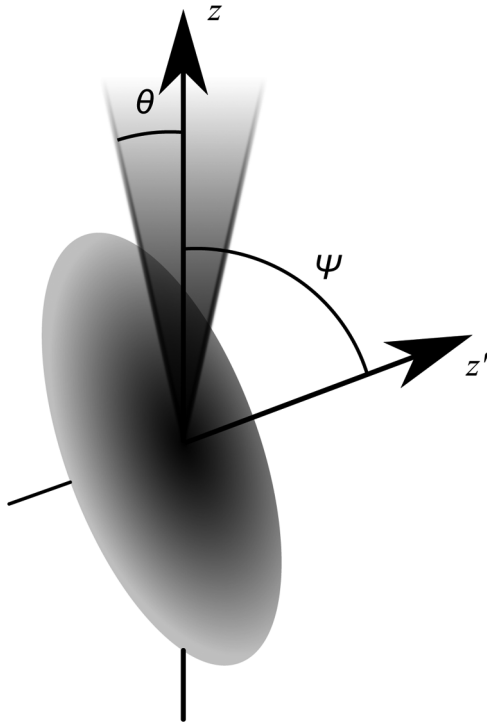


Fig. 2 Optical model of a platelet (oblate spheroid). Incident radiation propagates along the z -axis, z' is the symmetry axis of spheroid, Ψ is the angle between axes z and z' , and θ is the polar scattering angle.

radiation or 12 dipoles per a thickness of the spheroid when it was smaller than the wavelength in order to more precisely describe the shape of the platelet. The integration over φ was performed from 0 deg to 360 deg with 32 steps. To estimate the accuracy of the DDA simulations we increased the number of dipoles per wavelength to 40 for six typical LSPs. Based on the proven convergence of the DDA results to the exact value with refining discretization,²⁹ we used these simulations as a reference against which to test the standard DDA simulations. The ratio of the corresponding error norm to the norm of the whole LSP, both defined by Eq. (2), was smaller than 0.7% for these six cases.

The T-matrix approach is faster but does not converge for large aspect ratio.³⁰ However, we also tested the T-matrix method with discrete sources,³¹ which, unlike the conventional T-matrix method, can handle particles with highly nonspherical

geometries.³² In particular, we used null-field method with discrete sources (NFM-DS) package v.1.1 by Schmidt et al.³³ The agreement between the two methods was fine for some values of the model parameters, especially for relatively small platelets [Fig. 3(a)]. However, the accuracy of the NFM-DS deteriorated with increasing platelet volume. In the region of platelets with typical volume and large aspect ratio it showed unsatisfactory results [Fig. 3(b)], even with the number of multipoles (N_{rank}) two times larger than the value recommended in the supporting documentation supplied by the program. We contribute the difference between the two curves in Fig. 3(b) to the NFM-DS, because the estimated DDA errors are much smaller (see above). Moreover, the DDA was well tested against independent methods in this range of size and refractive index^{34,35} and, in particular, for red blood cells,^{35,36} while the T-matrix and similar methods are expected to suffer increasing numerical instability with increasing particle size.³⁷

3 Solution of the Inverse Light-Scattering Problem with PreComputed Database

3.1 Database Construction

We calculated the database consisting of $N = 500,000$ theoretical LSPs with parameters randomly distributed in the intervals shown in Table 1.

Random sampling of the database elements from a space of model parameters has several features compared to a regular grid. Firstly, it automatically accounts for different sensitivity of LSP to model parameters. For example, consider an artificial example, when one model parameter is irrelevant (LSP is completely independent of it), but this is unknown *a priori*. Then a regular grid will lead to redundant multiple calculations of the same LSPs, while random sampling will be equivalent to manual exclusion of irrelevant parameter and random sampling from the space of remaining parameters. Secondly, size of the randomly sampled database can be easily increased by an arbitrary number of elements, which is especially convenient for adaptive construction of the database.³⁸ Finally, formulae for statistical analysis of characterization results (Sec. 3.3) are rather simple.

All simulations were run on the compute cluster of the supercomputing center of the Novosibirsk State University. Typical simulation time of single LSP for a platelet is 1 min on a single core of Intel X5355 processor (2.66 GHz).

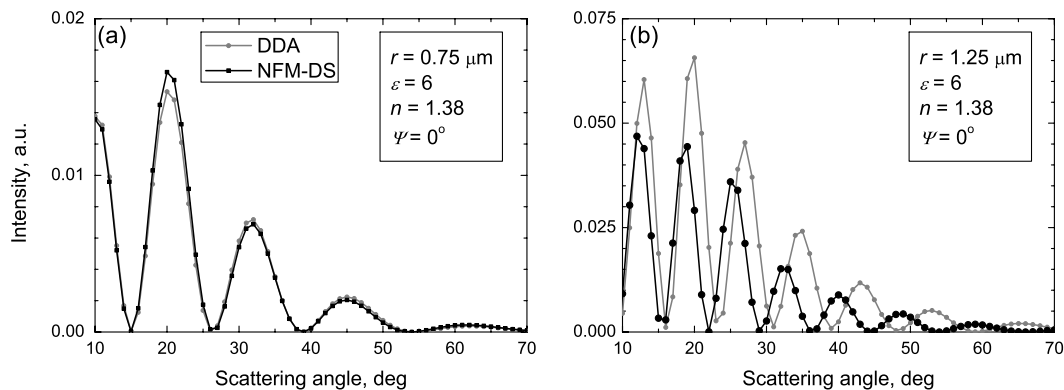


Fig. 3 Weighted LSPs [Eqs (1) and (3)] for two platelet models calculated from the discrete-dipoles approximation and the null-field method with discrete sources for (a) small and (b) typically sized platelets with relatively large aspect ratio $\varepsilon = 6$.

Table 1 Boundaries of the LSP database for oblate spheroids utilized in the solution of the inverse light-scattering problem.

Parameter of the spheroid	Lower limit	Upper limit
Equal volume sphere radius r	0.5 μm	2 μm
Aspect ratio ε	1	8
Refractive index n	1.35	1.5
Orientation angle Ψ	0 deg	90 deg

3.2 Global Optimization

In this and in the next section we develop a general method to solve the inverse light-scattering problem for nonspherical particles described by a few parameters. This method utilizes the ideas originally proposed in Ref. 21, which we adapt to use in discrete global optimization with a database of solutions of the direct light-scattering problem. Additionally, we analyze all related uncertainties.

The problem is transformed into the global minimization of the weighted sum of squares:

$$S(\boldsymbol{\beta}) = \|I_{\text{exp}} - I(\boldsymbol{\beta})\|^2 = \sum_{j=1}^k w(\theta_j) [I_{\text{exp}}(\theta_j) - I(\theta_j, \boldsymbol{\beta})], \quad (2)$$

where $\boldsymbol{\beta} = (r, \varepsilon, n, \Psi)$ is a vector of $p = 4$ model parameters, $I(\boldsymbol{\beta})$ and I_{exp} are a theoretical and an experimental LSP, respectively, k is a number of LSP points, $w(\theta)$ is the weighting function to reduce the effect of noise on the fitting results:²¹

$$w(\theta) = \frac{1^\circ}{\theta} \exp[-2 \ln^2(\theta/54 \text{ deg})]. \quad (3)$$

Equation (2) also defines the norm (distance) in the k -dimensional space of LSPs, which is further elaborated in Appendix.

We consider a general definition of a precalculated database, as a set $\{\boldsymbol{\beta}_i, p_i, I(\boldsymbol{\beta}_i)\}$, $i = 1, \dots, N$. Values p_i are relative probabilities (or weights) of database elements, which are defined normalized by $\sum_{i=1}^N p_i = 1$, and are determined by a structure of the database. For a particular case of random sampling (Sec. 3.1), $p_i = 1/N$. Another important case follows from deterministic division of the initial region of particle parameters \mathbf{B} (with the volume V) into nonoverlapping subregions V_i with $\boldsymbol{\beta}_i \in V_i$, then $p_i = V_i/V$. For example, this case applies to the global-optimization method DiRect, thus this paper can be considered a generalization of the approach proposed in Ref. 21.

Once the database is calculated, processing of any experimental LSP is performed by comparison with all LSPs from the database, i.e., the inverse problem is solved by nearest-neighbor interpolation on the database, using distance defined by Eq. (2). In addition to approximately finding a global minimum of $S(\boldsymbol{\beta})$ with the best estimate $\boldsymbol{\beta}_0$, it provides an approximate description of the whole surface of $S(\boldsymbol{\beta})$ by a set of values $[S(\boldsymbol{\beta}_i)]$.

3.3 Errors of Parameters Estimates

Bayesian approach is used to calculate a probability density function $P(\boldsymbol{\beta})$ over parameter space for a given experimental LSP:

$$P(\boldsymbol{\beta}) = \kappa S(\boldsymbol{\beta})^{-k_{\text{eff}}/2}, \quad \kappa = \left[\int_{\mathbf{B}} S(\boldsymbol{\beta})^{-k_{\text{eff}}/2} d\boldsymbol{\beta} \right]^{-1}, \quad (4)$$

where \mathbf{B} is a region in parameter space occupied by the database and $k_{\text{eff}} < k$ is an effective number of degrees of freedom, which is used to approximately compensate for correlation between neighboring residuals. It is determined by the structure of $I_{\text{exp}} - I(\boldsymbol{\beta}_0)$, see Ref. 21 for details.

The function $P(\boldsymbol{\beta})$ provides a complete description of the information deduced from an experimental LSP. In particular, one can calculate a mathematical expectation of any quantity $f(\boldsymbol{\beta})$:

$$\langle f(\boldsymbol{\beta}) \rangle = \int_{\mathbf{B}} f(\boldsymbol{\beta}) P(\boldsymbol{\beta}) d\boldsymbol{\beta}. \quad (5)$$

Since $S(\boldsymbol{\beta})$ is known in a set of points $\boldsymbol{\beta}_i$ with weights p_i , the integral can be approximated by a discrete sum, as a ratio of two sample means:

$$\langle f(\boldsymbol{\beta}) \rangle \approx \bar{g}/\bar{h}, \quad \bar{x} \equiv \frac{1}{N} \sum_{i=1}^N x_i, \quad g_i = f(\boldsymbol{\beta}_i) h_i, \quad (6)$$

$$h_i = N p_i S(\boldsymbol{\beta}_i)^{-k_{\text{eff}}/2},$$

which is valid for both random and deterministic sampling. The sample $h = \{h_i\}$ contains all known information about $P(\boldsymbol{\beta})$, and \bar{h} is an estimate of $1/\kappa$. One can also estimate the uncertainty of Eq. (6) using common statistical formulae:

$$\text{Var}[\bar{x}] = \frac{\text{Var}[x]}{N} \approx \frac{\text{SV}[x]}{N}, \quad (7)$$

$$\text{SV}[x] = \frac{1}{N-1} \sum_{i=1}^N (x_i - \bar{x})^2,$$

where $\text{Var}[\dots]$ denotes (unknown) population variance, and $\text{SV}[\dots]$ —a sample variance. Assuming \bar{g} and \bar{h} to be independent, which is always asymptotically correct for $N \rightarrow \infty$, we obtain:

$$\frac{\text{Var}[\langle f(\boldsymbol{\beta}) \rangle]}{\langle f(\boldsymbol{\beta}) \rangle^2} = \frac{1}{N} \left(\frac{\text{SV}[g]}{\bar{g}^2} + \frac{\text{SV}[h]}{\bar{h}^2} \right). \quad (8)$$

According to Eq. (6) we calculate the mathematical expectation $\boldsymbol{\mu} = \langle \boldsymbol{\beta} \rangle$ (generally different from $\boldsymbol{\beta}_0$) and the covariance matrix $\mathbf{C} = \langle (\boldsymbol{\beta} - \boldsymbol{\mu})(\boldsymbol{\beta} - \boldsymbol{\mu})^T \rangle$. One can also obtain highest-posterior density (HPD) confidence regions, defined as $\mathbf{R}(P_0) = \{\boldsymbol{\beta} | P(\boldsymbol{\beta}) > P_0\}$. P_0 is a variable threshold, which is implicitly determined by the confidence level α :

$$\alpha = \int_{\mathbf{R}(P_0)} P(\boldsymbol{\beta}) d\boldsymbol{\beta} \approx \kappa \sum_{\boldsymbol{\beta}_i \in \mathbf{R}(P_0)} p_i S(\boldsymbol{\beta}_i)^{-k_{\text{eff}}/2}. \quad (9)$$

It is important to note that the accuracy of determination of \mathbf{C} , and hence of HPD confidence regions, largely depends on accuracy of $S(\boldsymbol{\beta}_0)$. The latter can be thought of as an expected change of $S(\boldsymbol{\beta}_0)$ if the whole database is randomly resampled. When database is large enough $S(\boldsymbol{\beta}_0)$ is close to the result of exact fit $S(\boldsymbol{\beta}_\perp)$, which is determined solely by experimental noise for a particular processed LSP (see Appendix). In that case the accuracy of $S(\boldsymbol{\beta}_0)$ is fine (see Sec. 5.1). However, when theoretical testing LSP is processed (see Sec. 4), $S(\boldsymbol{\beta}_\perp) = 0$

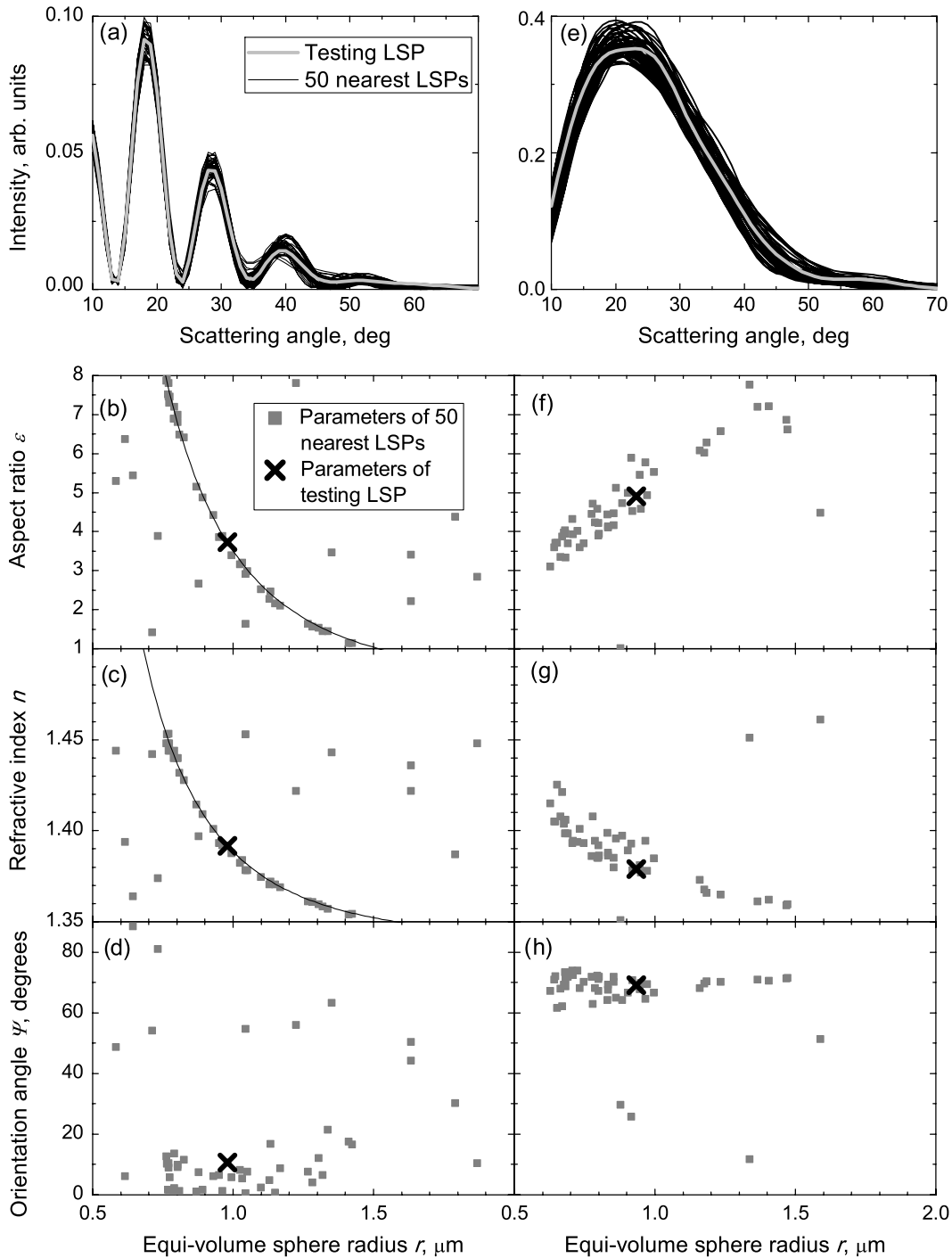


Fig. 4 (a) and (e) Testing weighted LSPs (gray curves) and 50 nearest from the database (black curves). (b) to (d) and (f) to (h) Projections of parameters of 50 nearest LSPs from the database (gray points). Black points indicate true parameters of testing LSPs. Solid lines on (b) and (c) are $\text{const} \times r^{-3}$ curves passing through parameters of testing LSPs (see Sec. 4).

and variance of $S(\beta_0)$ is large for any size of the database. Thus, the proposed method to estimate characterization uncertainties is inadequate for and cannot be tested with theoretical LSPs without noise.

4 Testing of the Database

In order to estimate the validity of our approach, we performed database testing with 1000 additionally calculated LSPs, hereinafter named testing LSPs. Parameters of testing LSPs were

randomly sampled from \mathbf{B} (same as for the database). Each testing LSP was processed by the database, determining the best estimate β_0 , which was then compared with true (reference) parameter values β_r .

Unfortunately, resulting β_0 were sometimes quite far from β_r . For instance, 90% of testing LSPs have a distance between r_0 and r_r less than 10% of the sampling range, while others have larger distances, up to 52% of the range (data not shown). Results for the other 3 parameters are similar. This indicates a presence of identical or very similar LSPs with largely different parameters. In

order to study this issue, we plotted parameters of 50 nearest LSPs from the database for each testing LSP, since HPD confidence regions cannot be determined unambiguously (Sec. 3.3). In Fig. 4, two typical cases are shown: orientation angle $\Psi < 40$ deg (left column) and >50 deg (right column). Note that here and further we present weighted LSPs, i.e., those multiplied by the weighting function [Eq. (3)].

When $\Psi < 40$ deg, the LSPs are nearly identical [Fig. 4(a)] and corresponding points evidently group into compact curves, at least in the $r\varepsilon$ - and εn -planes [Fig. 4(b) and 4(c)]. We found that these curves are well described by the equations

$$\begin{aligned} r\varepsilon^{1/3} &= a = \text{const} \\ r(n - n_0)^{1/3} &= \text{const} \Rightarrow r\varepsilon^{-2/3}(n - n_0) = b(n - n_0) = \text{const}, \end{aligned} \quad (10)$$

where n_0 is the refractive index of the medium, and a and b denote larger and smaller axis of spheroid, respectively. The corresponding isolines passing through β_r are shown in Fig. 4(b) and 4(c).

Equation (10) can be explained in the framework of the anomalous diffraction approximation (ADA), in which an LSP depends only on projection of a particle on a plane, perpendicular to the incident propagation direction, and maximal phase shift.³⁹ By design, the ADA is applicable to optically soft ($n - n_0 \ll n_0$) particles much larger than the wavelength. This condition is generally not satisfied for blood platelets because their size is not that large. Nevertheless, LSPs calculated with the ADA agrees well with the DDA calculations for $\Psi = 0$ deg [Fig. 5(a)]. And in this case, Eq. (10) is equivalent to constancy of the projection area and the phase shift. For the general case $\Psi \neq 0$ deg the projection area equals $\pi a^2 f$ and the phase shift $-b(n - n_0)/f$, where the factor f is⁴⁰

$$f = \sqrt{\cos^2 \beta + \frac{\sin^2 \beta}{\varepsilon^2}}. \quad (11)$$

Curves in the $r\varepsilon$ - and εn -planes are well described by the relations in Eq. (10) while f is close to unity, which takes place for $\Psi < 40$ deg (e.g., $f = 0.87$ for $\Psi = 30$ deg and $\varepsilon = 4$).

The phenomenon of parameter compensation also takes place for $\Psi > 50$ deg, producing almost identical LSPs [Fig. 4(e)]. In this case, compact curves are also evident, although not so narrow. However, we could not explain it by

a simple argument. ADA is obviously inapplicable in this case [Fig. 5(b)]. Potentially, one of other existing approximations for optically soft particles⁴¹ can solve this puzzle. However, the phenomenon may also be associated with integration over the azimuthal angle in Eq. (1). In other words, in some cases a complete 2D distribution of light-scattering intensity varied along the confidence curves (data not shown), but not the resulting LSP. Finally, we note that anti-correlation between r and n [Fig. 4(c) and 4(g)] can be considered fundamental, since the combination of these two parameters determines the overall intensity of a LSP. It becomes a major factor when fitting LSPs with little oscillatory structure, such as in Fig. 4(e).

Described parameters compensation is beautiful from a theoretical viewpoint, but awful from a practical one, since it results in huge uncertainties of determined platelet characteristics. Alleviating this problem is possible using additional *a priori* information on the platelet parameters. The first candidate for such correction is the refractive index: the range [1.35, 1.5] used for the database is very large, covering all conceivable values. There are, however, methods to evaluate the blood platelets refractive index, in particular, 2-angle light-scattering ADVIA-120 hematology system. This device measures the mean platelet component (MPC), which is proportional to the refractive index, employing isovolumetric spheroiding of cells.⁴² It was shown that the MPC depends on the particular anticoagulant and platelets activation state. In sodium citrate resting platelets had MPC of 25.7 ± 0.9 g/dl (as mean \pm SD) and after addition of thrombin, 21.9 ± 1.9 g/dl.⁴³ Doubling SD, this corresponds to 95% confidence intervals for the refractive index of [1.380, 1.387] and [1.370, 1.383], respectively. Therefore, restricting the refractive index to the narrow range of [1.37, 1.39] seems reasonable, and we use it to alleviate the problem of parameter compensation. Although previous study of blood platelets with the SFC²³ reported much wider range, [1.36, 1.45], it is plagued by large errors of individual cell measurements, in addition to other drawbacks described in Sec. 1. Finally, we note that restricting the refractive index effectively decreases the number of used database elements to about 65,000.

5 Experimental Results and Discussion

5.1 Verification of the Assumption about the Refractive Index

In order to estimate an adequacy of the database size N , we conducted the following virtual experiment. First, we performed

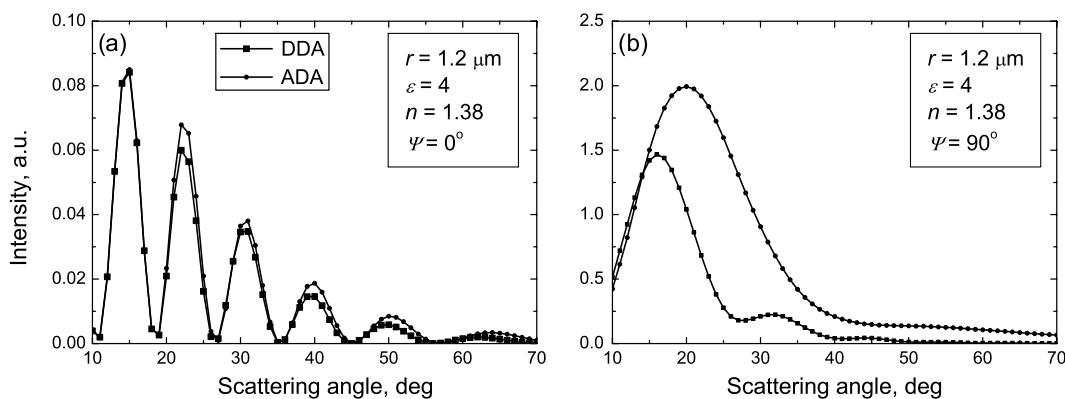


Fig. 5 Weighted LSPs for a typical model of a typical platelet calculated with discrete-dipoles approximation and anomalous diffraction approximation for orientation angle (a) $\Psi = 0$ deg and (b) $\Psi = 90$ deg.

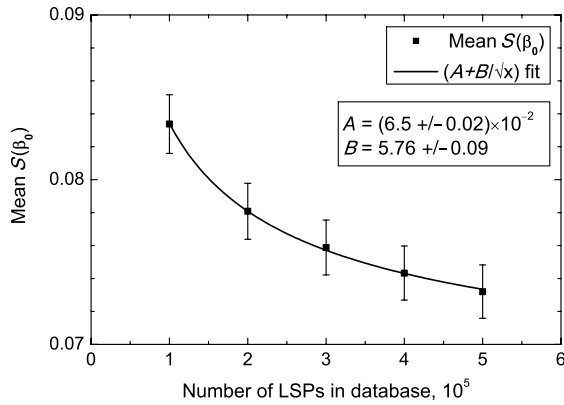


Fig. 6 Dependence of the average over sample best-fit value $S(\beta_0)$ on the database size for experimental LSPs. The coefficients A and B are obtained by fitting with the theoretical curve (see Appendix) are also shown as values \pm standard errors.

global optimization with the complete database containing $N = 5 \times 10^5$ LSPs, and obtained a set of N values $[S(\beta_i)]$. Then, we calculated the quantity $s(Q) = \min_{i \leq Q} S(\beta_i)$, which is equal to values of $S(\beta_0)$ obtained by global optimization with first Q LSPs from the database. These quantities were then averaged over all experimental LSPs, and are shown in Fig. 6 varying Q from 10^5 to 5×10^5 with a step of 10^5 . Theoretical dependence of $\langle s(Q) \rangle$ on the database size Q is given by (A7). This analysis allows us to fit the points in Fig. 6 by a theoretical curve and determine the asymptotic value $A = \lim_{Q \rightarrow \infty} \langle s(Q) \rangle = 6.5 \times 10^{-2}$, which is a measure of the experimental noise, i.e., deviation of experimental LSPs from theoretical model of oblate spheroid. The remaining deviation due to sparsity of the database $[s(Q) - A]$ is only 0.8×10^{-2} for the largest Q , which is much smaller than the level of the experimental noise. Hence, further increase of the database size should not significantly change the results. The same analysis applies to any part of the database with proportional scaling of Q and N , because of the random sampling used for its construction.

We also examined the errors of Monte Carlo integration [Eq. (8)] that also depends on N . Using the complete database,

the statistical errors for evaluation of μ and C were not larger than 0.5%.

5.2 Verification of the Assumption about the Refractive Index

In order to verify the validity of restricting the refractive index, we performed several tests, carrying out global optimization with the complete and truncated (i.e., with the refractive index restricted to the range [1.37, 1.39]) databases.

First, for each experimental LSP we determined whether the HPD 95%-confidence region (using the complete database, see Sec. 3.3), or more specifically its projection on the axis of refractive index, intercepts the range [1.37, 1.39]. This condition implies that the hypothesis of restricted refractive index is acceptable in the probabilistic sense with 95% probability. We found that the interception take place for the vast majority (93%) of platelets LSPs. For the remaining 7% of platelets the restriction of the refractive index also produces adequate results, so we did not exclude them from considerations.

Second, we examined a best-fit weighted sum of squares $S(\beta_0)$. Distributions of platelets LSPs over $S(\beta_0)$ are shown in Fig. 7 for both complete and truncated databases. The distributions are well-described by log-normal curves, and corresponding fit parameters are shown in each plot. One can see that the restriction of the refractive index only slightly deteriorates the agreement between the theoretical and experimental LSPs.

5.3 Typical Results of Global Optimization

Projections of HPD confidence region obtained by global optimization with the complete and truncated databases for the typical experimental LSP are shown on Fig. 8. Regions on the upper panel follow the same pattern as the clouds of 50 nearest parameters in Sec. 4 (cf., right column of Fig. 4). The LSP itself is shown in Fig. 9 together with the best-fit LSPs from the complete and truncated databases. $S(\beta_0)$ is slightly larger for the truncated database, as expected. However, the corresponding best-fit LSP visually seems more appropriate, i.e., better describes the second maxima. This illustrates one of the promising future directions of research: replacing weighted sum of

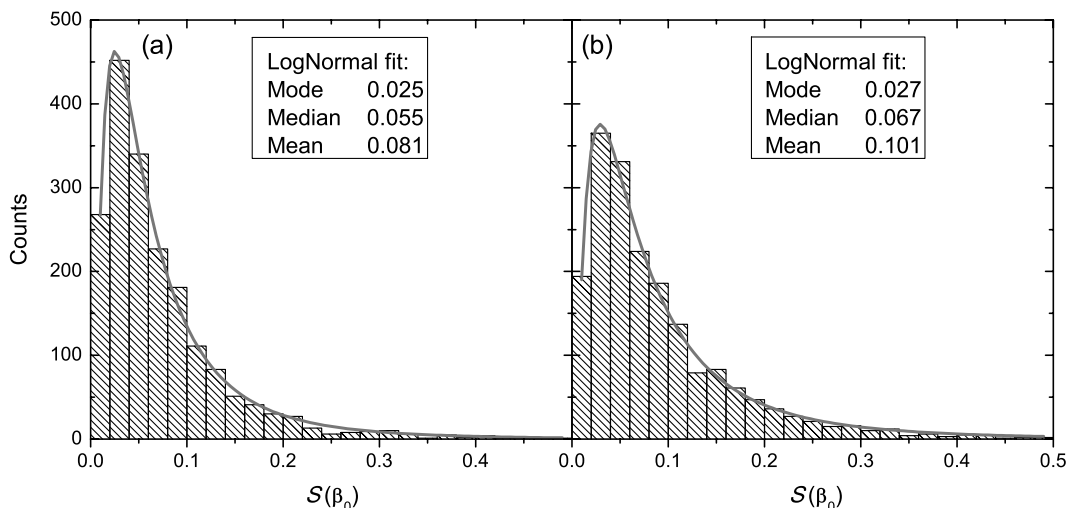


Fig. 7 Distributions over best-fit weighted sum of squares $S(\beta_0)$ for (a) the complete database and for (b) the database with refractive index restricted to the range [1.37, 1.39]. Results of the lognormal fit (mode, median, and mean values for log-normal distributions) are shown.

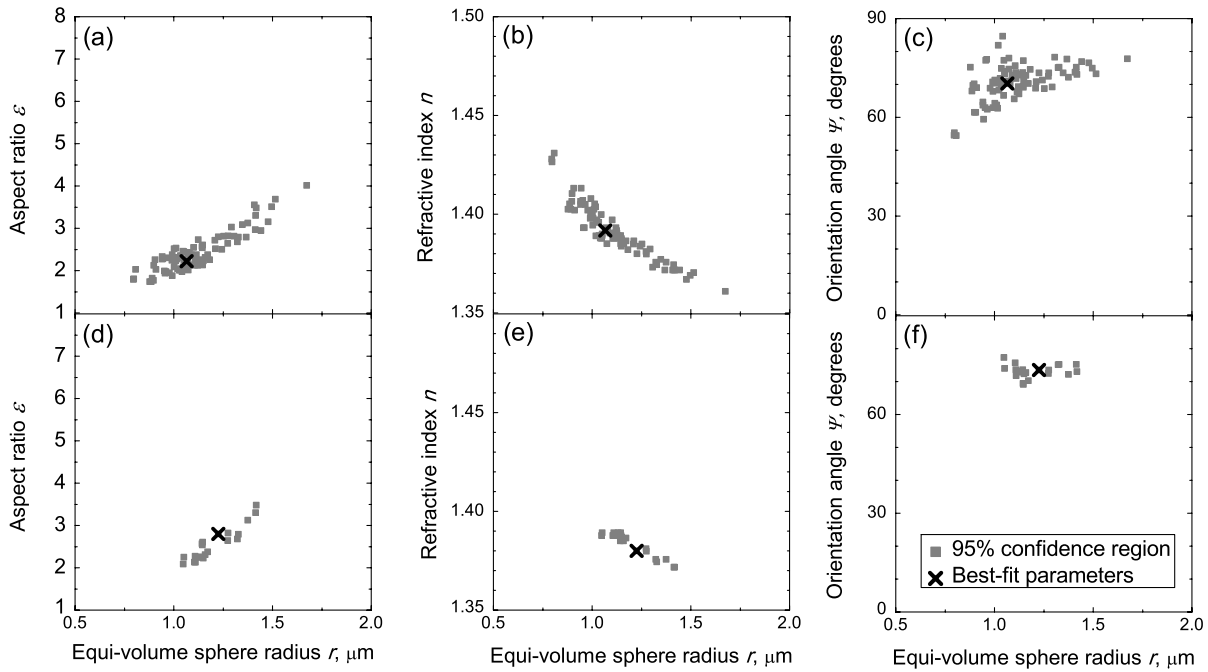


Fig. 8 Projections of 95%-confidence region for a typical experimental LSP for (a) to (c) the complete and (d) to (f) truncated databases.

squares by a more physically based distance measure, e.g., based on explicit consideration of the positions of LSP extrema. Anyway, the main effect of restricting the refractive index, as shown in Fig. 9, is the decrease of the uncertainties of parameter estimates by a factor from 1.3 to 2 (while for some other LSPs uncertainties decreased 14-fold for aspect ratio and 5-fold for equi-volume sphere radius), which was our design goal. This effect is also demonstrated through constriction of confidence regions in Fig. 8.

The following results were obtained using the truncated database. In particular, Fig. 10 presents characterization results for four typical blood platelets that were chosen based on their $S(\beta_0)$, cf., Fig. 7(b). We emphasize the precision of determined r (median uncertainty is 125 nm, while for 35% of platelets) less than 100 nm, which is very good for optical methods. This corresponds to a median precision of 0.9 fl for the platelet volume in the wide range of platelet aspect ratios. The precision of the

aspect ratio is 0.62 (median) and <0.3 for 23% of platelets. Distributions of the platelet sample over uncertainties of parameters are approximately log-normal (data not shown). Large uncertainties between platelet variations of the parameter can be caused by several factors, including varying signal-to-noise ratio of the measured LSP and varying deviations of the real platelet shape from the oblate spheroid model.

5.4 Results of Characterization of Blood Platelet Population

In Fig. 11 we present obtained results of characterization (best-fit values) for resting platelets (left column) and platelets activated by 10 μM ADP (right column). In particular, maps of platelet volume versus aspect ratio are shown in Fig. 11(a) and 11(b). The area of platelets evidently moves to the region of the smaller aspect ratio. The corresponding distributions over

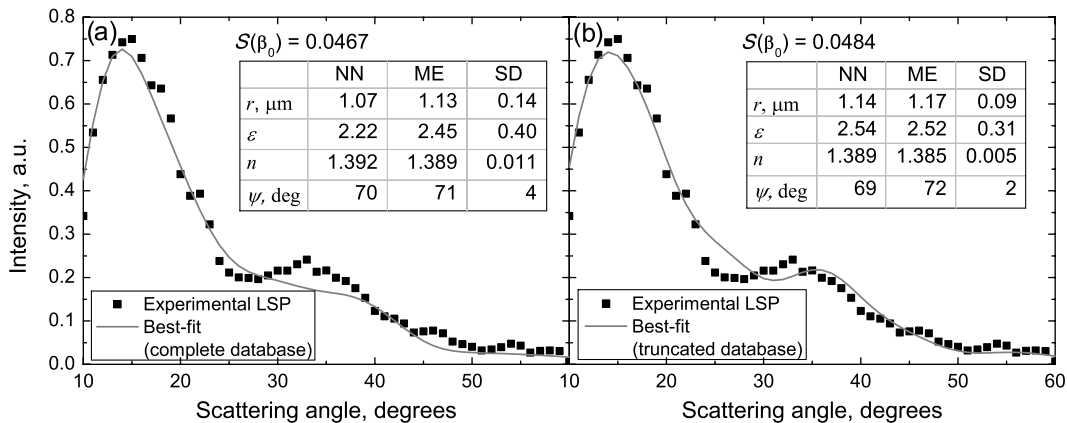


Fig. 9 Typical experimental LSP (dots) and best-fit LSPs (gray lines) obtained with (a) the complete database and (b) the database with the refractive index restricted to the range [1.37, 1.39]. Results of global optimization, including parameters of the nearest LSP from the database (NN), mathematical expectation (ME), and standard deviation (SD) of parameters are also shown.

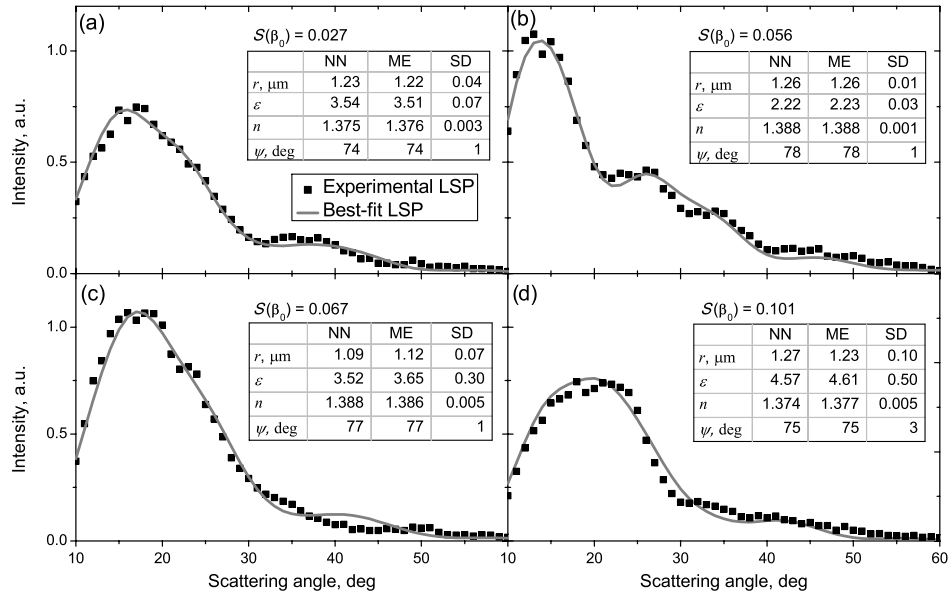


Fig. 10 Typical experimental and best-fit theoretical LSPs as obtained by global optimization using the database with restricted refractive index. Parameters of the nearest LSP from the database (NN), mathematical expectation (ME), and standard deviation (SD) of parameters are shown in inset tables.

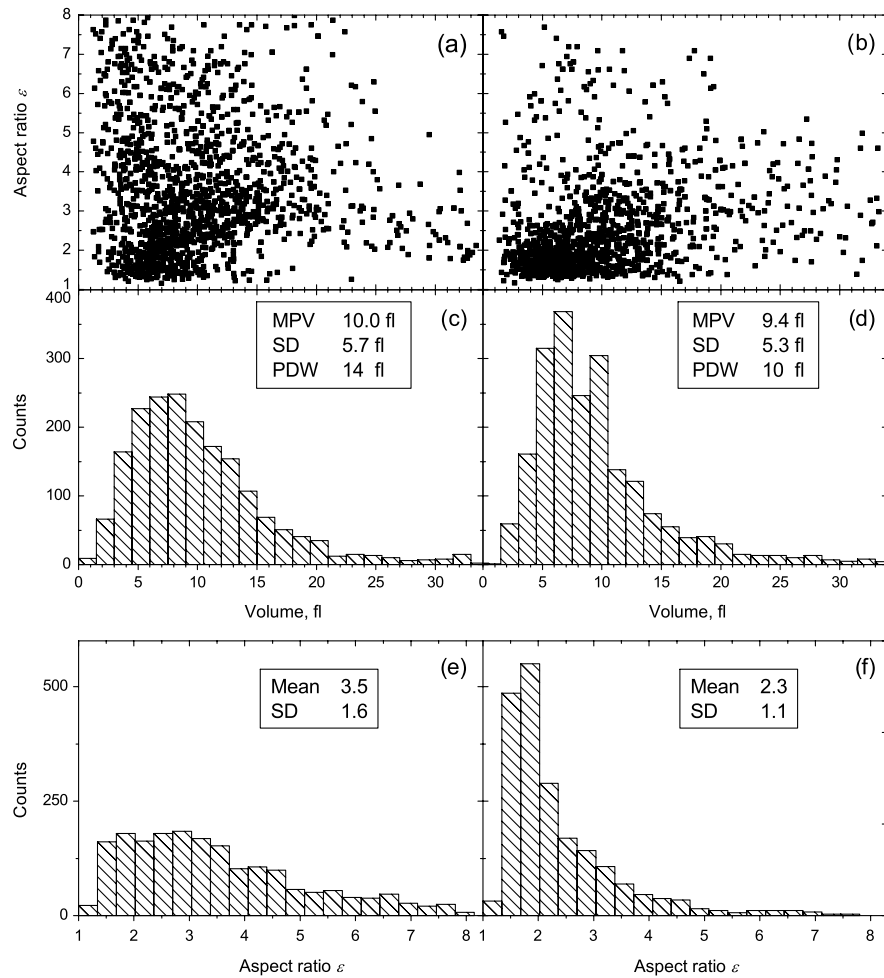


Fig. 11 Maps of blood platelet volume versus aspect ratio (best-fit values) for (a) native sample (1883 cells) and (b) after the addition of $10 \mu\text{M}$ ADP (2050 cells). Distributions over a volume and an aspect ratio for [(c) and (e)] resting and [(d) and (f)] activated platelets are shown, respectively.

the platelet volume [Fig. 11(c) and 11(d)] are in a qualitative agreement with the conventional curves measured by Coulter counters. Mean platelet volume (MPV) values of 10.0 and 9.4 fl for resting and activated platelets, respectively, fall within the reference range of 8 to 12 fl. MPV for activated platelets is slightly less, which can be supported by the phase-contrast microscopic measurements¹⁷ and centrifugal volumetric experiments,⁴⁴ although the statement that the platelet volume increases during activation is more generally accepted.² Platelet distribution width, defined as width at the level of 20% of maximal peak, is also within the reference range of 9 to 14 fl for both cases.

Distributions over the aspect ratio (best-fit values) for both resting and activated platelets are shown in [Fig. 11(e) and 11(f)]. The first distribution shows a peak with a relatively large amount of platelets with aspect ratio near 2, although, according to the literature, such platelets are a minor part in the normal state.⁵ It can be explained by the fact that platelets are partly activated, which always occurs during blood collecting and preparation of a platelet-rich plasma. This is supported by the fact that after addition of 10 μM ADP almost all platelets transfer to that peak, leaving a little trace in the region of aspect ratio >2 , corresponding to unactivated platelets or platelets which shape is still changing.

6 Conclusion

We developed a general approach for characterization of non-spherical particles from experimental angle-resolved LSPs using a precomputed database of theoretical LSPs. This method can be applied to characterize particles which shape can be described by several parameters. It provides the best-fit parameters for each experimental LSP, as well as uncertainties of the estimates (or the complete covariance matrix) and HPD confidence regions.

This method was applied for characterization of individual blood platelets modeled as an oblate spheroid described by three morphological characteristics and orientation angle. The database of 500,000 theoretical LSPs was constructed. Testing of the database revealed a phenomenon of parameter compensation, resulting in nearly identical LSPs with substantially different parameters. The majority of LSPs are determined only by three combinations of parameters rather than by all four parameters. This was partly explained in the framework of anomalous diffraction approximation. A general method to overcome the parameter compensation is to measure additional experimental signals, e.g., azimuthal distribution of light-scattering intensity^{45,46} or additional Mueller matrix elements (i.e., polarization of scattered light). Actually, we are permanently improving the SFC technology with measurement of two-dimensional⁴⁷ and polarized LSPs that provides determination of six characteristics of a particle from light scattering.²⁵ However, these improvements lead to the more complex SFC operation that increases a cost of analysis.

The developed method was tested on a blood sample of a healthy donor, resulting in good agreement with the literature data. Clinically important parameters, namely the mean platelet volume (MPV) and the platelet distribution width (PDW), were both within the reference ranges. Moreover, the median precision of individual volume measurements is 0.9 fl, based on the internal estimate of parameter uncertainties. Aspect ratios of native platelets were 3.5 ± 1.5 (as mean \pm SD), although the distribution was bimodal, showing a population of platelets

with aspect ratio near 2. We believe this population to be spontaneously activated platelets. It is partly confirmed by the fact that after addition of 10 μM ADP most platelets move into this region of the distribution, having aspect ratio of 2.3 ± 1.1 . While direct comparisons with independent measurements are required to reveal the real potential of the presented method, it may find use for accurate evaluation of platelet volume and shape and for label-free detection of activated platelets.

Appendix

To study the effect of the database sparsity on best-fit $S(\beta_0)$, [Eq. (2)] let us additionally define β_\perp : the result of exact fit (e.g., by a long run of the global optimization) for the same I_{exp} . In other words, $I(\beta_\perp)$ is the nearest to I_{exp} element from the model manifold $L = \{I(\beta) | \beta \in \mathbf{B}\}$ or the foot of perpendicular from I_{exp} onto L . Illustration of these definitions is given in Fig. 12. Assuming smallness of $\gamma = \beta_0 - \beta_\perp$, we linearize $I(\beta)$ near β_\perp :

$$I(\beta_0) \approx I(\beta_\perp) + \sum_{\mu=1}^p J_\mu \gamma_\mu, \quad J_\mu = \frac{\partial I(\beta_\perp)}{\partial \beta_\mu}, \quad (12)$$

where J_μ is the Jacobian (gradient) of I at β_\perp . Equation (12) is justified, since we are interested only in the main asymptotic term for $N \rightarrow \infty$. By definition of J_μ and β_\perp , $[J_\mu, I_{\text{exp}} - I(\beta_\perp)] = 0$, where the inner product (\cdot, \cdot) is defined according to Eq. (2). Therefore, $S(\beta_0)$ is expressed as:

$$S(\beta_0) \approx \left\| \sum_{\mu=1}^p J_\mu \gamma_\mu \right\|^2 + S(\beta_\perp) = \sum_{\mu, \nu=1}^p T_{\mu\nu} \gamma_\mu \gamma_\nu + S(\beta_\perp), \quad (13)$$

$$T_{\mu\nu}(\beta_\perp) = (J_\mu, J_\nu).$$

The goal of this appendix is to evaluate $S(\beta_0)$ as a function of the database size Q . More specifically, we need to average $S(\beta_0)$ over many experimental LSPs, which can be considered as averaging over β_\perp with a certain probability density. The latter is usually poorly known, but we assume that it is a smooth distribution with a sufficiently broad support in \mathbf{B} to cover a lot of database elements. This assumption is valid both for experiment in Sec. 5.1 and for testing theoretical LSPs in Sec. 4. Then the averaged $S(\beta_0)$ should not depend on a particular realization of

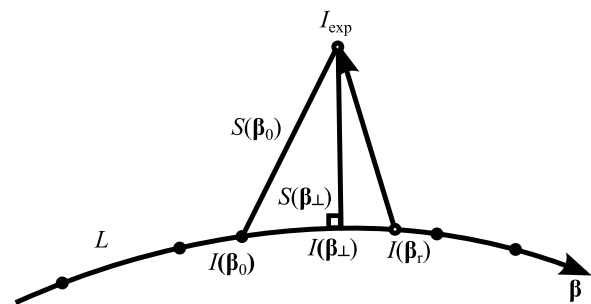


Fig. 12 Illustration of global optimization with the precomputed database in the case of $k = 2$, $p = 1$. L is a p -dimensional model manifold, in which filled points denote database elements. The ideal (reference) platelet LSP $I(\beta_\perp)$ and actually measured one I_{exp} (with added noise) are shown by empty points. $I(\beta_0)$ is a nearest LSP from the database, while $I(\beta_\perp)$ is the foot of the perpendicular from I_{exp} onto L .

the database (for a given size), or equivalently it should not change if it is additionally averaged over all possible realizations of the database, i.e., over all possible locations of best-fit element β_0 . This together with Eq. (13) imply

$$\begin{aligned} \langle S(\beta_0) \rangle_{\perp} &\approx \langle \langle S(\beta_0) \rangle_{\perp} \rangle_0 = \langle \langle S(\beta_0) \rangle_0 \rangle_{\perp} \\ &\approx \left\langle \sum_{\mu,\nu=1}^p T_{\mu\nu} \langle \gamma_{\mu}\gamma_{\nu} \rangle_0 \right\rangle_{\perp} + \langle S(\beta_{\perp}) \rangle_{\perp}, \end{aligned} \quad (14)$$

where subscripts \perp and 0 denote averaging over β_{\perp} and β_0 , respectively. The order of averaging was changed due to their independence, and we used that $T_{\mu\nu}$ and $S(\beta_{\perp})$ do not depend on β_0 . The only remaining Q -dependent term is $\langle \gamma_{\mu}\gamma_{\nu} \rangle_0$, which is mostly determined by the local density of the database near β_{\perp} . Unless β_{\perp} is close to boundaries of \mathbf{B} , the result should not depend on a particular shape of \mathbf{B} . Thus, for simplicity we consider \mathbf{B} to be a sphere with radius r_0 centered at β_{\perp} .

Then the probability density of γ is isotropic, hence

$$\langle \gamma_{\mu}\gamma_{\nu} \rangle_0 = \langle |\gamma|^2 \rangle_0 \delta_{\mu\nu} / p. \quad (15)$$

The uniform density of database elements in \mathbf{B} implies that probability of $|\gamma|$ to be from r to $r + dr$ is as follows:

$$\begin{aligned} P(r) &= -\frac{d}{dr} \left(1 - \frac{V(r)}{V(r_0)} \right)^Q \\ &= \left(1 - \frac{V(r)}{V(r_0)} \right)^{Q-1} \frac{Q}{V(r_0)} \frac{dV(r)}{dr}, \end{aligned} \quad (16)$$

where $V(r)$ is volume of p -dimensional sphere with radius r . Therefore,

$$\begin{aligned} \langle |\gamma|^2 \rangle_0 &= \int_0^{r_0} dr P(r) r^2 = Q r_0^2 \int_0^1 du (1-u)^{Q-1} u^{2/p} \\ &= Q r_0^2 B\left(\frac{2}{p} + 1, Q\right) \approx r_0^2 \Gamma\left(\frac{2}{p} + 1\right) Q^{-2/p}, \end{aligned} \quad (17)$$

where $u = V(r)/V(r_0) = (r/r_0)^p$ and the asymptotic property of beta function for large Q was used.

Finally, we substitute Eqs. (17) and (15) into Eq. (14) and obtain

$$\begin{aligned} \langle S(\beta_0) \rangle_{\perp} &\approx \langle S(\beta_{\perp}) \rangle_{\perp} + \frac{r_0^2}{p} \Gamma\left(\frac{2}{p} + 1\right) Q^{-2/p} \langle \|\mathbf{J}(\beta_{\perp})\|^2 \rangle_{\perp} \\ &= A + B Q^{-2/p}, \quad \|\mathbf{J}\|^2 = \sum_{\mu=1}^p T_{\mu\mu}, \end{aligned} \quad (18)$$

where A is a measure of the experimental noise, which is zero for theoretical testing LSPs. On the contrary, B is mostly determined by the fundamental properties of L and is effected by a particular set of experimental (or testing) LSPs only through the probability density of β_{\perp} .

Acknowledgments

This work was supported by the program of the Russian Government, "Research and educational personnel of innovative Russia" (Contracts P1039, P422, 14.740.11.0921, 8752, 14.B37.21.0457, and 8804), by a grant from the Government of Russian Federation 11.G34.31.0034, by the Program of the

President of the Russian Federation for State Support of the Leading Scientific Schools (grant NSh-65387.2010.4), and by the Russian Foundation of Basic Research (grant 12-04-00737-a).

References

1. A. D. Michelson, *Platelets*, 2nd ed., A. D. Michelson, Ed., Academic Press, San Diego (2006).
2. A. R. L. Gear and R. K. Polanowska-Grabowska, "The platelet shape change," in *Platelets in Thrombotic and Non-Thrombotic Disorders*, P. Greslele, C. P. Page, V. Fuster, and J. Vermynen, Eds., pp. 319–337, Cambridge University Press, Cambridge (2002).
3. J. F. David-Ferreira, "The blood platelet: electron microscopic studies," *Int. Rev. Cytol.* **17**, 99–148 (1964).
4. M. M. Frojmovic and J. G. Milton, "Human platelet size, shape, and related functions in health and disease," *Physiol. Rev.* **62**(1), 185–261 (1982).
5. M. M. Frojmovic and R. Panjwani, "Geometry of normal mammalian platelets by quantitative microscopic studies," *Biophys. J.* **16**(9), 1071–1089 (1976).
6. A. Mathur and J. F. Martin, "Platelet heterogeneity: physiology and pathological consequences," in *Platelets in Thrombotic and Non-Thrombotic Disorders*, P. Greslele, C. P. Page, V. Fuster, and J. Vermynen, Eds., pp. 70–79, Cambridge University Press, Cambridge (2002).
7. R. D. Eastham, "Rapid whole-blood platelet counting using an electronic particle counter," *J. Clin. Pathol.* **16**(2), 168–169 (1963).
8. J. Paulus, "Platelet size in man," *Blood* **46**(3), 321–336 (1975).
9. N. B. Grover et al., "Electrical sizing of particles in suspensions," *Biophys. J.* **9**(11), 1398–1414 (1969).
10. K. Y. Kim, K. E. Kim, and K. H. Kim, "Mean platelet volume in the normal state and in various clinical disorders," *Yonsei Med. J.* **27**(3), 219–226 (1986).
11. S. J. Shattil, M. Cunningham, and J. A. Hoxie, "Detection of activated platelets in whole blood using activation-dependent monoclonal antibodies and flow cytometry," *Blood* **70**(1), 307–315 (1987).
12. J. Dachary-Prigent et al., "Annexin V as a probe of aminophospholipid exposure and platelet membrane vesiculation: a flow cytometry study showing a role for free sulfhydryl groups," *Blood* **81**(10), 2554–2565 (1993).
13. L. Pearson et al., "A rapid flow cytometric technique for the detection of platelet-monocyte complexes, activated platelets and platelet-derived microparticles," *Int. J. Lab. Hematol.* **31**(4), 430–439 (2009).
14. L. C. Baker et al., "Flow cytometric assays to detect platelet activation and aggregation in device-implanted calves," *J. Biomed. Mater. Res.* **41**(2), 312–321 (1998).
15. E. Maurer-Spurej and K. Chipperfield, "Past and future approaches to assess the quality of platelets for transfusion," *Transfus. Med. Rev.* **21**(4), 295–306 (2007).
16. R. D. Allen et al., "Transformation and motility of human platelets: details of the shape change and release reaction observed by optical and electron microscopy," *J. Cell Biol.* **83**(1), 126–142 (1979).
17. J. G. Milton and M. M. Frojmovic, "Turbidometric evaluations of platelet activation: relative contributions of measured shape change, volume, and early aggregation," *J. Pharmacol. Methods* **9**(2), 101–115 (1983).
18. G. V. Born et al., "Quantification of the morphological reaction of platelets to aggregating agents and of its reversal by aggregation inhibitors," *J. Physiol. (Lond.)* **280**, 193–212 (1978).
19. V. P. Maltsev, "Scanning flow cytometry for individual particle analysis," *Rev. Sci. Instrum.* **71**(1), 243–255 (2000).
20. V. P. Maltsev and K. A. Semyanov, *Characterisation of Bio-Particles from Light Scattering*, VSP, Utrecht (2004).
21. D. I. Strokotov et al., "Is there a difference between T- and B-lymphocyte morphology?," *J. Biomed. Opt.* **14**(6), 064036 (2009).
22. A. I. Konokhova et al., "Light-scattering flow cytometry for identification and characterization of blood microparticles," *J. Biomed. Opt.* **17**(5), 057006 (2012).
23. I. V. Kolesnikova et al., "Determination of volume, shape and refractive index of individual blood platelets," *J. Quant. Spectrosc. Radiat. Transfer* **102**(1), 37–45 (2006).

24. M. B. Zucker and J. Borrelli, "Reversible alterations in platelet morphology produced by anticoagulants and by cold," *Blood* **9**(6), 602–608 (1954).
25. D. I. Strokotov et al., "Polarized light-scattering profile—advanced characterization of nonspherical particles with scanning flow cytometry," *Cytometry A* **79**(7), 570–579 (2011).
26. C. F. Bohren and D. R. Huffman, *Absorption and Scattering of Light by Small Particles*, Wiley, New York (1983).
27. M. A. Yurkin and A. G. Hoekstra, "The discrete dipole approximation: an overview and recent developments," *J. Quant. Spectrosc. Radiat. Transfer* **106**(1–3), 558–589 (2007).
28. M. A. Yurkin and A. G. Hoekstra, "The discrete-dipole-approximation code ADDA: capabilities and known limitations," *J. Quant. Spectrosc. Radiat. Transfer* **112**(13), 2234–2247 (2011).
29. M. A. Yurkin, V. P. Maltsev, and A. G. Hoekstra, "Convergence of the discrete dipole approximation. I. Theoretical analysis," *J. Opt. Soc. Am. A* **23**(10), 2578–2591 (2006).
30. M. I. Mishchenko, L. D. Travis, and D. W. Mackowski, "T-matrix computations of light scattering by nonspherical particles: a review," *J. Quant. Spectrosc. Radiat. Transfer* **55**(5), 535–575 (1996).
31. A. Doicu, T. Wriedt, and Y. A. Eremin, *Light Scattering by Systems of Particles: Null-Field Method with Discrete Sources: Theory and Programs*, Springer, Berlin (2006).
32. J. Hellmers, V. Schmidt, and T. Wriedt, "Improving the numerical stability of T-matrix light scattering calculations for extreme particle shapes using the nullfield method with discrete sources," *J. Quant. Spectrosc. Radiat. Transfer* **112**(11), 1679–1686 (2011).
33. A. Doicu, T. Wriedt, and Y. A. Eremin, "NFM-DS," (2010), <http://www.scattport.org/index.php/programs-menu/t-matrix-codes-menu/239-nfm-ds> (21 December 2012).
34. M. A. Yurkin, V. P. Maltsev, and A. G. Hoekstra, "The discrete dipole approximation for simulation of light scattering by particles much larger than the wavelength," *J. Quant. Spectrosc. Radiat. Transfer* **106**(1–3), 546–557 (2007).
35. M. A. Yurkin et al., "Systematic comparison of the discrete dipole approximation and the finite difference time domain method for large dielectric scatterers," *Opt. Express* **15**(26), 17902–17911 (2007).
36. K. V. Gilev et al., "Comparison of the discrete dipole approximation and the discrete source method for simulation of light scattering by red blood cells," *Opt. Express* **18**(6), 5681–5690 (2010).
37. W. R. C. Somerville, B. Auguie, and E. C. Le Ru, "Severe loss of precision in calculations of T-matrix integrals," *J. Quant. Spectrosc. Radiat. Transfer* **113**(7), 524–535 (2012).
38. K. V. Gilev et al., "An optimization method for solving the inverse Mie problem based on adaptive algorithm for construction of interpolating database," *J. Quant. Spectrosc. Radiat. Transfer*, in press.
39. H. C. van de Hulst, *Light Scattering by Small Particles*, Dover, New York (1981).
40. G. J. Streekstra et al., "Light scattering by red blood cells in ektacytometry: Fraunhofer versus anomalous diffraction," *Appl. Opt.* **32**(13), 2266–2272 (1993).
41. S. K. Sharma and D. J. Somerford, *Light Scattering by Optically Soft Particles: Theory and Applications*, Springer-Verlag, Berlin (2006).
42. M. G. Macey et al., "Use of mean platelet component to measure platelet activation on the ADVIA 120 haematology system," *Cytometry* **38**(5), 250–255 (1999).
43. C. E. Ahnadi et al., "Assessment of platelet activation in several different anticoagulants by the Advia® 120 Hematology System, fluorescence flow cytometry, and electron microscopy," *Thromb. Haemostasis* **90**(5), 940–948 (2003).
44. G. V. R. Born, "Observations on the change in shape of blood platelets brought about by adenosine diphosphate," *J. Physiol.* **209**(2), 487–511 (1970).
45. E. Hirst et al., "A method for investigating the orientational behaviour of fibrous particles in gaseous flow," *Part. Syst. Charact.* **12**(1), 3–9 (1995).
46. M. Giacomelli et al., "Size and shape determination of spheroidal scatterers using two-dimensional angle resolved scattering," *Opt. Express* **18**(14), 14616–14626 (2010).
47. G. V. Dyatlov et al., "The scanning flow cytometer modified for measurement of two-dimensional light-scattering pattern of individual particles," *Meas. Sci. Technol.* **19**(1), 015408 (2008).